Frontiers of Information Technology & Electronic Engineering
www.zju.edu.cn/jzus; engineering.cae.cn; www.springerlink.com
ISSN 2095-9184 (print); ISSN 2095-9230 (online)
E-mail: jzus@zju.edu.cn

Torque characteristics in a large permanent magnet synchronous generator with stator radial ventilating air ducts*

He HAO[1], Wei-zhong FEI[†‡2], Dong-min MIAO[1], Meng-jia JIN[1], Jian-xin SHEN[1]

([1]*College of Electrical Engineering, Zhejiang University, Hangzhou 310027, China*)

([2]*Power Engineering Centre, Cranfield University, Cranfield MK43 0AL, UK*)

[†]E-mail: w.fei@cranfield.ac.uk

Received July 24, 2015; Revision accepted Feb. 17, 2016; Crosschecked July 13, 2016

Abstract: In this study, we investigated the torque characteristics of large low-speed direct-drive permanent magnet synchronous generators with stator radial ventilating air ducts for offshore wind power applications. Magnet shape optimization was used first to improve the torque characteristics using two-dimensional finite element analysis (FEA) in a permanent magnet synchronous generator with a common stator. The rotor step skewing technique was then employed to suppress the impacts of mechanical tolerances and defects, which further improved the torque quality of the machine. Comprehensive three-dimensional FEA was used to evaluate accurately the overall effects of stator radial ventilating air ducts and rotor step skewing on torque features. The influences of the radial ventilating ducts in the stator on torque characteristics, such as torque pulsation and average torque in the machine with and without rotor step skewing techniques, were comprehensively investigated using three-dimensional FEA. The results showed that stator radial ventilating air ducts could not only reduce the average torque but also increase the torque ripple in the machine. Furthermore, the torque ripple of the machine under certain load conditions may even be increased by rotor step skewing despite a reduction in cogging torque.

Key words: Permanent magnet synchronous generator (PMSG), Radial ventilating air duct, Torque ripple, Step skewing, Magnet shape optimization, Finite element analysis, Wind power

http://dx.doi.org/10.1631/FITEE.1500238 **CLC number:** TM351

1 Introduction

The market of low-speed rare-earth permanent magnet synchronous generators (PMSGs) for large offshore direct-drive wind power applications is gradually increasing as a result of their distinctive merits including excellent torque/power density, high efficiency, compactness, low maintenance and hence high reliability (Tapia *et al.*, 2013). However, the nonexistence of mechanical gears suggests that the undesirable effects of torque pulsation generated on the rotor of a large PMSG are unattenuated. Therefore, effective reduction on the torque pulsations in such large direct-drive PMSGs must be carried out to prevent hazardous mechanical vibration (Sopanen *et al.*, 2011). There have been many recent studies of torque ripple and its reduction in permanent magnet (PM) brushless machines. Torque ripple reduction methods can typically be divided into two categories from machine design and control perspectives (Jahns and Soong, 1996). The machine design based methods are normally less costly but

‡ Corresponding author

* Project supported by the National Natural Science Foundation of China (No. 51377140) and the National Basic Research Program (973) of China (No. 2013CB035604)

ORCID: He HAO, http://orcid.org/0000-0001-6376-9106

more effective than the control based ones (Fei *et al.*, 2012). Thus, to mitigate cogging torque, deleterious harmonic content of the back electromotive force (EMF) and hence electromagnetic torque pulsations of PM brushless machines, various machine design techniques have been proposed, including magnet profiling (Islam *et al.*, 2005; Fei and Luk, 2009; Chen NN *et al.*, 2010), magnet segmentation (Lateb *et al.*, 2006; Boukais and Zeroug, 2010; Ashabani and Mohamed, 2011), magnet pole arc width optimization (Li and Slemon, 1988; Zhu and Howe, 2000; Bianchi and Bolognani, 2002; Yang *et al.*, 2006; Fei and Luk, 2010), magnet pole pairing (Bianchi and Bolognani, 2002; Wang *et al.*, 2010; Fei and Luk, 2012), and stator slot and rotor pole number combinations (Atallah *et al.*, 2003; Han *et al.*, 2010; Güemes *et al.*, 2011). A common and effective technique to reduce torque ripple in PM brushless machines is rotor step skewing (Zhu *et al.*, 2005; Islam *et al.*, 2009; Chen HS *et al.*, 2010; Güemes *et al.*, 2011), which is often employed along with other methods to suppress the impacts of mechanical tolerances and defects in large machines. However, all the above approaches result in additional complexity and reduced torque output.

The heat dissipation efficiency from the active material of a PMSG in a large offshore wind power application generally determines its overall torque capacity. To manage the stator temperature effectively within a safe range, air ducts with a radial ventilating configuration are commonly implemented to guide the forced air transflux and remove the heat generated by losses during the machine operation (Pyrhonen *et al.*, 2010). Hence, the stator is divided axially into a number of sub-stacks by such air ducts that change the effective length in the axial direction and affect the back EMF and synchronous inductances of the machine (Ruuskanen *et al.*, 2011). The magnetic fringing effects in these air ducts impose a noticeable impact on the stator flux density distributions, especially in the axial direction. Therefore, more severe magnetic saturations occur on the ends of the sub-stacks. However, such magnetic saturations affect the torque characteristics of high power PMSGs including torque pulsation and average output torque. Therefore, it is important to investigate comprehensively the impacts of these air ducts on the torque characteristics. Comprehensive three-dimensional (3-D) finite element analysis (FEA) is very useful for reliable predictions of those effects. However, 3-D FEA models for such large PMSGs are usually of high complicacy and computational intensity. Therefore, an approximate 3-D FEA method has been proposed to reduce significantly the computational time without noticeably compromising accuracy (Fei *et al.*, 2013).

This study focused on the improvement and investigation of the torque characteristics, including torque pulsation and average output torque, of a large low-speed direct-drive PMSG with stator radial ventilating air ducts for offshore wind power applications. The results of this study will show that the cogging torque and electromagnetic torque pulsation of the machine can be significantly mitigated by magnet shape optimization. Moreover, the radial ventilating air ducts in the stator result in increased on-load torque ripple with reduced average torque in the machine. Note that the on-load torque ripple in the machine with optimal magnet design may even be increased by rotor step skewing. However, rotor step skewing is practically essential to alleviate the impact of mechanical tolerances and defects on the torque characteristics of such large machines.

2 Direct-drive PMSG for offshore wind turbines

2.1 PMSG configuration

An integral-slot surface-mounted PMSG with the conventional one slot per pole per phase configuration, which can accommodate single-layer modular windings with high packaging and fundamental winding factors, is a very promising candidate for high-performance applications such as large offshore direct-drive wind power generations. The generator considered in this study was a large 4.5 MW PMSG with 360 stator slots and 120 rotor magnet poles for offshore wind power application. The open slot configuration, which can easily accommodate the modular coils, was implemented in order to considerably improve the overall winding process and package factor. Furthermore, the double air cooling configuration with several air ducts in the stator is one of the most effective thermal management techniques for such a large-scale PMSG (Ruuskanen *et al.*, 2013). Generally, such an air duct number is typically around 20, and they account for about seven percent of the overall stator axial

length. Hence, the stator of the proposed PMSG consists of 24 sub-stacks with 74 mm axial length and 23 6-mm radial ventilating air ducts in-between. The actual arrangement of the sub-stacks and radial ventilating air ducts is depicted in the schematic axial cross-section of the machine in Fig. 1, while the main design parameters of the proposed PMSG are given in Table 1. As the rated operational speed of the machine is quite low at 15 rad/min (15 Hz electrical frequency), lamination sheets of silicon steel type 65ww470 were employed for the stator cores, and high-strength rare-earth neodymium-iron-boron (NEOMAX-35H) magnets were chosen to achieve high torque density.

Table 1 Main parameters of the proposed PMSG

	Machine parameter	Value
Rotor geometry	Rotor inner diameter (mm)	4230
	Rotor yoke width (mm)	60
	Magnet width (mm)	103
	Magnet height (mm)	19
	Airgap length (mm)	6
	Rotor pole number	120
Stator geometry	Stator inner diameter (mm)	4400
	Stator outer diameter (mm)	4900
	Stator yoke width (mm)	50
	Slot height (mm)	200
	Coil height (mm)	190
	Stator slot opening (mm)	19
	Stator effective axial length (mm)	1876
	Stator total axial length (mm)	1914
	Stator slot number	360
Winding data	Slot wind layer number	1
	Coil number in series	3
	Turn number per coil	18
	Rated electrical frequency (Hz)	15
	Rated current (peak) (A)	5778

2.2 Magnet shape optimization

The considerable slot opening effects due to the open slots normally consort with considerable cogging torque and on-load electromagnetic torque pulsation, especially in the proposed PMSG with a one slot per pole per phase configuration. The magnets in the machine were mounted directly on the surface of rotor iron. Hence, a magnet optimization scheme was implemented in the machine to minimize the cogging torque, belt back EMF harmonics, and hence the overall on-load electromagnetic torque pulsations. Although the conventional sinusoidal magnet shaping scheme can effectively alleviate the cogging torque and torque ripple, the corresponding fundamental back EMF and hence torque would be significantly compromised (Pang *et al.*, 2005).

In this study, a new magnet shape optimization scheme was therefore implemented to enhance the electromagnetic torque without compromising the cogging torque and torque ripple in the proposed PMSG. A schematic of the proposed magnet shape scheme is depicted in Fig. 2. The magnet is flat at the bottom to facilitate manufacture and assembly. The magnet height H at width W can be expressed as

$$H=\begin{cases} H_{\mathrm{pm}}, & W\le W_{\mathrm{pmc}},\\ H_{\mathrm{pm}}-H_{\mathrm{m}}\cos\dfrac{(W-W_{\mathrm{pmc}})\pi}{2(W_{\mathrm{m}}-W_{\mathrm{pmc}})}, & W_{\mathrm{pmc}}<W\le W_{\mathrm{pm}},\\ 0, & W_{\mathrm{pm}}<W, \end{cases} \tag{1}$$

where W_{pmc} is the width of the central part of the magnet with a height of H_{pm}, H_{m} is the difference between the maximum and minimum magnet heights over one whole pole, W_{pm} is the width of the magnet, and W_{m} is the maximum magnet width over one pole, which can be easily obtained as

$$W_{\mathrm{m}}=2(R_{\mathrm{ro}}-H_{\mathrm{m}})\sin\frac{\pi}{p}, \tag{2}$$

where R_{ro} is the outer radius of the rotor and p is the rotor magnet pole number. A fairly small H_{m} is normally required to achieve a reasonable electromagnetic torque with minimized cogging torque and torque ripple. To simplify the optimization, only W_{pm} and W_{pmc} were optimized to improve the

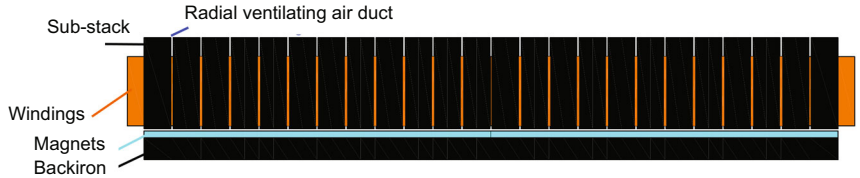

Fig. 1 Schematic axial cross-section of the PMSG with radial ventilating air ducts in the stator

machine torque characteristics, with a fixed H_{m} of 11 mm and unchanged stator, by comprehensive 2-D FEA. Both open-circuit and rated load field analyses were carried out to obtain the cogging torque, overall torque ripple, and average torque. The peak-to-peak (P-P) values of the cogging torque in the machine are plotted in Fig. 3a, which shows that the cogging torque could be effectively minimized by combinations of W_{pm} and W_{pmc}. Generally, a large W_{pm} is preferred to deliver high torque with a low cogging torque. The P-P torque ripple and average torque from the rated load conditions are shown in Figs. 3b and 3c, respectively. The average toque improves as W_{pm} and W_{pmc} increase. However, the torque ripple would become severe as W_{pmc} rises. Fig. 3 clearly implies that a compromise must be made among cogging torque, torque ripple, and average toque, to achieve the optimal goal. Thus, 10 mm and 103 mm were chosen for the optimal W_{pm} and W_{pmc}, respectively, by taking into account all three features.

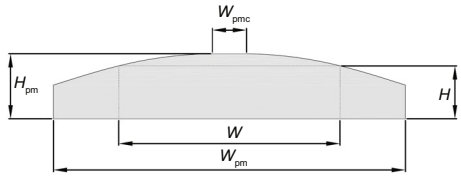

Fig. 2 Sketch of the magnet shape scheme

2.3 Effective axial length

A traditional PM machine has only two end areas, whose effects on machine performance can normally be neglected in 2-D FEA. However, each air duct in the stator of the proposed PMSG constitutes two extra end surface areas for respective stator substacks. The fringing effects on those end areas will inevitably place impacts on the machine characteristics, especially axial ones, and must be taken into account. Therefore, the inclusion of the effective axial length of the machine is essential for an accurate prediction by 2-D FEA. The effective axial length should be able to provide a correct main flux calculation with 2-D FEA.

In this study, open-circuit 2-D and 3-D FEA were carried out to obtain the effective axial length of the machine. Fig. 4 depicts the optimal machine with flux density distributions under open-circuit condition from respective 2-D and 3-D FEA results. Necessary boundary conditions are employed in both 2-D and 3-D FEA models to effectively reduce the corresponding model size and hence significantly save computational time. With anti-periodic and symmetric boundary conditions, 1/120 and 1/240 of the machine were modeled in 2-D and 3-D FEA, respectively. The effective axial length of the machine was derived as 1876 mm (98% of the overall stator length) for 2-D FEA to deliver the same fundamental flux

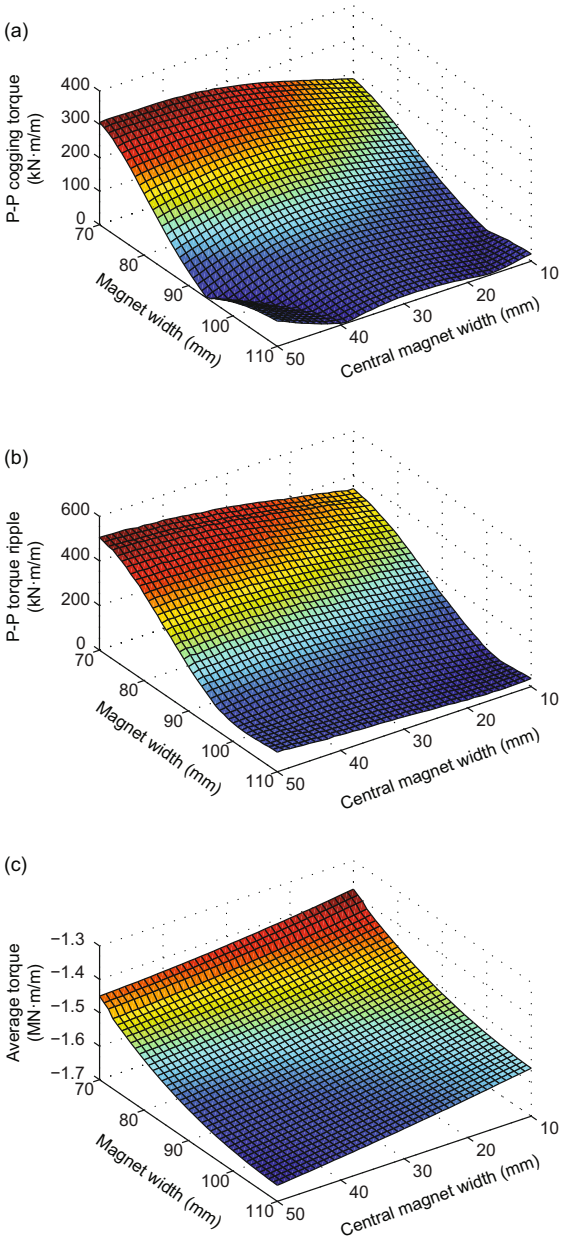

Fig. 3 The torque characteristics of the PMSG with magnet shape optimization from 2-D FEA results: (a) P-P cogging torque; (b) P-P torque ripple; (c) average rated torque

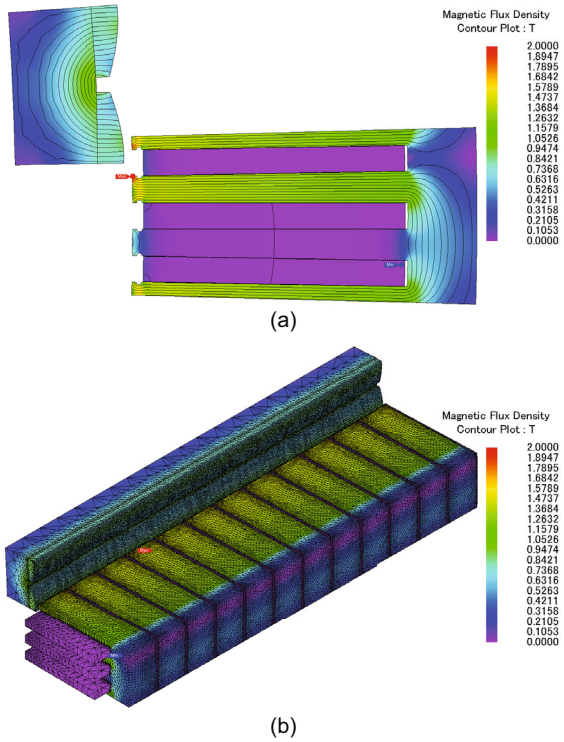

Fig. 4 Open-circuit flux density distribution of the proposed PMSG: (a) 2-D FEA; (b) 3-D FEA (References to color refer to the online version of this figure)

linkages as with 3-D FEA.

The corresponding cogging torque and phase back EMF waveforms were obtained by 2-D and 3-D FEA models. The cogging torque waveforms (Fig. 5) show that both the profiles and magnitudes are in very close agreement between the 2-D and 3-D FEA results. The magnet profiling scheme implemented has mitigated the cogging torque effectively. The results also imply the trivial impacts of the radial ventilating air ducts in the stator on the cogging torque. The resultant phase back EMF waveforms and their spectra were derived and compared (Fig. 6). The difference between the waveforms is barely noticeable (Fig. 6a) as their values of the fundamental component are the same. However, Fig. 6b shows that the 5th and 7th harmonics of the back EMF are almost eradicated in 2-D FEA results as a result of magnet optimization while they are still quite evident in 3-D FEA results due to the effects of the radial ventilating air ducts in the stator. The results show that the influences of the radial ventilating air ducts in the stator on the belt back EMF harmonics are quite noticeable, especially the fifth one, and are the main contributors of on-load electromagnetic torque pulsation in the proposed PMSG. Overall, the 2-D FEA approach with effective axial length can deliver quite accurate open-circuit characteristics of the machine.

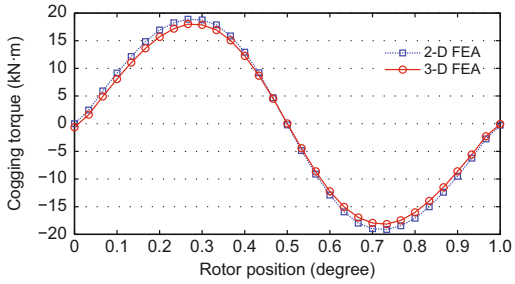

Fig. 5 Cogging torque waveforms of the optimal machine from 2-D and 3-D FEA results

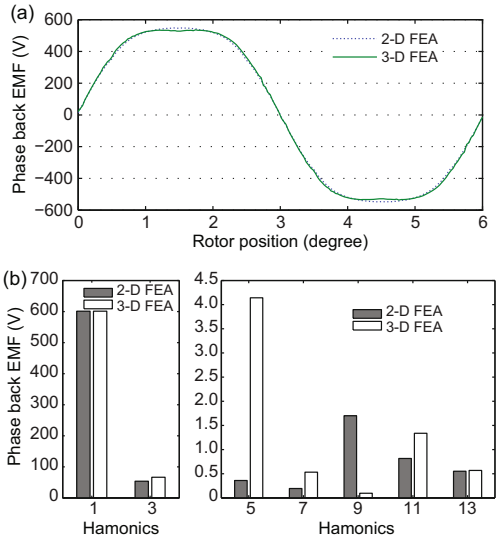

Fig. 6 2-D and 3-D FEA back EMF waveforms (a) and spectra (b) of the optimal machine

3 Torque characteristics of the optimal PMSG

For simplicity and clarity, balanced three-phase sinusoidal currents are assumed in the windings to decouple the nonlinear torque effects from the controller. The instantaneous torque of PM machines can be segregated into three components: cogging torque, reluctance torque, and PM torque. The cogging torque is independent of load conditions, while the reluctance torque and PM torque are highly dependent on the load conditions, such as the current magnitude and current phase advance angle. Without loss of generality, the instantaneous torque in the proposed PMSG with load conditions can be obtained by synthesizing the corresponding

load-dependent and load-independent components:

$$T(\theta)=\sum_{n=1}^{\infty}T_{cn}\sin(nN_{\mathrm{sr}}\theta)+\sum_{n=0}^{\infty}T_{en}(I_{\mathrm{p}},\varphi_{\mathrm{p}})\sin[3nN_{\mathrm{r}}\theta+\varphi_{en}(I_{\mathrm{p}},\varphi_{\mathrm{p}})], \tag{3}$$

where T_{cn} is the amplitude of the nth harmonic of the cogging torque, N_{sr} is the least common multiple of stator slot number N_{s} and rotor pole number N_{r}, and $T_{en}(I_{\mathrm{p}},\varphi_{\mathrm{p}})$ and $\varphi_{en}(I_{\mathrm{p}},\varphi_{\mathrm{p}})$ are the respective amplitude and phase angle of the nth harmonic of the electromagnetic torque generated by the phase current with amplitude I_{p} and phase φ_{p}. The frequencies of the cogging torque and electromagnetic torque pulsation harmonics are the same in the proposed machine.

The open-circuit back EMF results from the previous section imply that the 5th and 7th harmonics mainly contributed by the radial ventilating air ducts in the stator will result in extra components on the load-dependent electromagnetic torque pulsation of the proposed PMSG under load conditions. Consequently, the torque characteristics of the proposed machine excited by rated phase current with phase advance angles varying from −30° to 30° were comprehensively evaluated by 2-D and 3-D FEA. The torque waveforms from 2-D and 3-D FEA results are depicted in Figs. 7a and 7b respectively, and the corresponding magnitudes of the torque harmonics are derived and compared in Fig. 7c. The profile of the 2-D FEA torque waveform resembles its 3-D FEA counterpart with a lagged current phase angle applied. When the current phase angle turns into advanced, the waveforms start to diverge and the difference reaches its maximum at the phase advance angle that gives the lowest torque pulsation. With further increases in the phase advance angle, the waveforms gradually become similar once again. The 2-D FEA results overestimate the average torque values but underestimate the torque pulsations. On the whole, the accuracy of 2-D FEA predictions on the torque characteristic in the proposed optimal PMSG is indubitably challenged. The relative errors of the average torque and P-P value of torque ripple between 2-D and 3-D FEA results are shown in Fig. 8.

Fig. 8 shows that the relative errors for the average torque will steadily decay as the current advance angle rises. In order to use the whole envelope to the

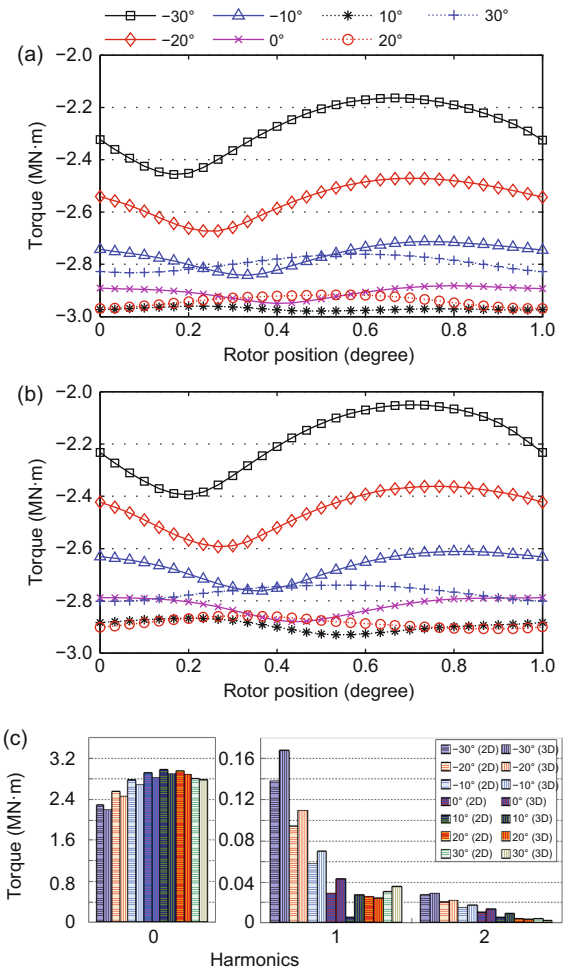

Fig. 7 2-D and 3-D FEA torque characteristics of the optimal machine: (a) torque waveforms from 2-D FEA; (b) torque waveforms from 3-D FEA; (c) torque harmonic magnitudes

utmost extent, moderate magnetic saturations are deliberately introduced in the proposed optimal machine with the rated load condition. As the current advance angle increases, the saturations in the stator will be accordingly alleviated thanks to the flux weakening effects. The end regions of sub-stacks in the actual stator experience more severe magnetic saturations than the corresponding center regions since the magnetic fringing effects occur in the related air ducts. Hence, the magnetic fields near these end regions will inevitably differ from the ones near the corresponding center regions, which is confirmed by the 3-D FEA field results in Fig. 8. Moreover, such differences will slowly diminish as the phase advance angle of the current increases from flux enhancement to flux weakening (Fig. 9). For simplicity, uniform flux density distributions are hypothesized

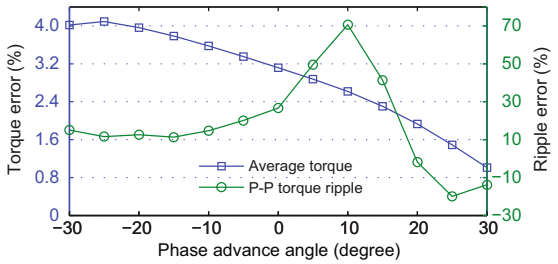

Fig. 8 Relative errors between 2-D and 3-D FEA results

along the axial direction of the machine for the 2-D FEA method. This assumption induces noticeably large errors on the average values of 2-D and 3-D FEA torque, especially when the phase advance angles are relatively small. However, such a relative error will be below 1.0% with 30° phase advance angle. The current phase advance angles from 2-D and 3-D FEA results delivering the maximum average torque in the proposed optimal PMSG are about 10° and 15°, respectively (Fig. 7). Since the predicted inductances from the 2-D FEA model are smaller than the 3-D FEA ones (Ruuskanen *et al.*, 2013), it will underestimate the reluctance torque contribution in the machine. This can partially explain the mismatch between the optimal 2-D and 3-D FEA values for the phase advance angle.

On the other hand, the 2-D FEA torque ripples in most cases are considerably lower than the 3-D FEA ones due to the underestimated 5th and 7th harmonics of the back EMF. The first and second harmonic components are the main contributors of the whole electromagnetic torque pulsation in the machine (Fig. 7). With the phase advance angle of the current beyond 20°, the relative errors on P-P values of torque ripple become negative (Fig. 8), which implies that the 2-D FEA method will overestimate the torque pulsation instead. The respective current phase advance angles from 2-D and 3-D FEA results delivering the minimum torque ripple about 10° and 20°. As for the average torque, the same explanations still serve the turn on the evident mismatches between the 2-D and 3-D FEA P-P values of torque ripple.

4 Optimal PMSG with rotor step skewing

Although the cogging torque and torque ripple of the proposed PMSG have been minimized by

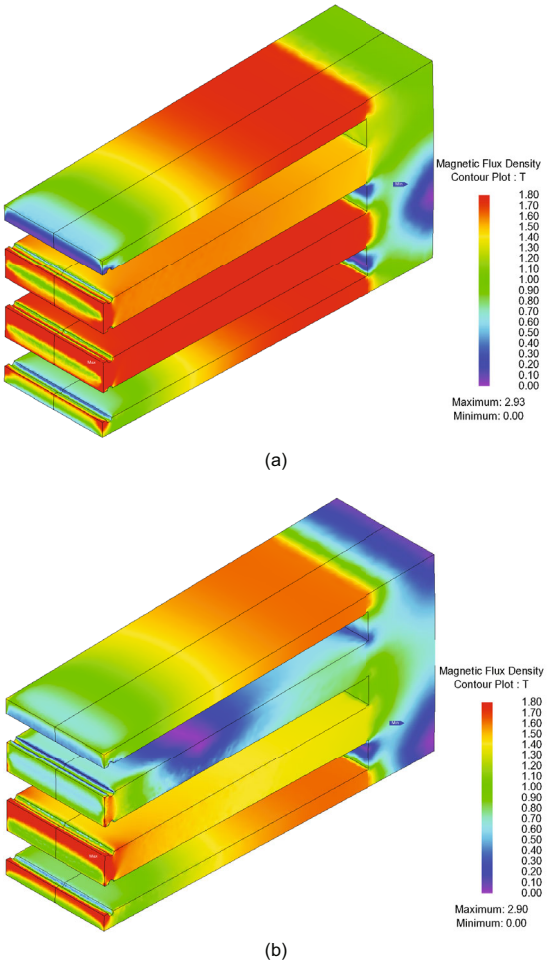

Fig. 9 3-D FEA flux density distributions on individual sub-stack of the stator excited by rated current with −30° (a) and 30° (b) phase advance angles (References to color refer to the online version of this figure)

magnet shape optimization, mechanical defects and tolerances are practically unavoidable in such large machines during manufacture and assembly. The rotor skewing technique is widely employed to alleviate the impacts of those factors. However, the magnets in the machine have flat bottoms. This would make continuous magnet skewing impractical as it would result in an irregular magnet shape and magnetization pattern. The rotor step skewing technique can be an effective alternative to resolve these issues. Therefore, synergy of magnet shape optimization and rotor step skewing is important for preventing severe mechanical vibration and acoustic noise in large PM wind generators (Sopanen *et al.*, 2011).

The machine with a rotor step skewing

technique can be essentially considered as a number of axially conjoined identical sub-machines with circumferentially and sequentially shifted rotors. By ignoring the end effects and axial interactions between the sub-machines, the overall instantaneous torque can be obtained by synthesizing the electromagnetic torque of all the individual sub-machines with the phase advancing concept (Islam *et al.*, 2009) as

$$\begin{aligned} T(\theta) = & \sum_{n=1}^{\infty} \frac{\sin\left(\frac{\upsilon}{2} n N_{\mathrm{sr}} \theta_{\mathrm{s}}\right)}{\upsilon \sin\left(\frac{1}{2} n N_{\mathrm{sr}} \theta_{\mathrm{s}}\right)} T_{cn} \sin\left(n N_{\mathrm{sr}} \theta\right) \\ & + \sum_{n=0}^{\infty} \sum_{k=0}^{\upsilon-1} \Big[\frac{1}{\upsilon} T_{en}\left(I_{\mathrm{p}}, \varphi_{\mathrm{p}} - \varphi_k\right) \\ & \cdot \sin(3 n N_{\mathrm{r}}\left(\theta + \varphi_k\right) + \varphi_{en}(I_{\mathrm{p}}, \varphi_{\mathrm{p}} - \varphi_k))\Big], \end{aligned} \tag{4}$$

where

$$\varphi_k = \frac{\upsilon - 2k - 1}{2} \theta_{\mathrm{s}}, \tag{5}$$

υ is the number of the skewing step, and θ_{s} is the actual mechanical angle of the skew between two adjacent modules. Obviously, all the harmonics in the load-independent cogging torque as the first item in Eq. (4) can be eradicated except those that are multiples of υ with the skewing angle as

$$\theta_{\mathrm{s}} = \frac{2k\pi}{\upsilon N_{\mathrm{sr}}}, \quad k = 1, 2, \ldots, \tag{6}$$

where k is usually set as small as possible to avoid severe performance degradation for the machine. However, the influence of rotor step skewing on the load-dependent component of the torque ripple is not very obvious from Eq. (4). Since the associations of the cogging torque to the overall torque pulsation in the proposed ideal machine are minimized by magnet shape optimization, the skewing angle could be different from that derived by Eq. (6) for improved overall torque ripple reduction (Chu and Zhu, 2013). However, inevitable mechanical defects in the actual machine could significantly increase the cogging torque, so the skewing angle from Eq. (6) is essential.

With the corresponding angles for the skewing step derived from Eq. (6), the PMSGs with up to four steps were comprehensively studied by both synthesized 2-D and 3-D FEA. The 3-D FEA open-circuit flux density distributions of the PMSG with the rotor step skewing technique are shown in Fig. 10. The resultant cogging torque (Fig. 11) and back EMF waveforms (Fig. 12) of the machine with rotor step skewing were derived and compared accordingly. Comparisons between Figs. 4 and 10 indicate that the cogging torque can be effectively mitigated and even almost eradicated when the rotor step number exceeds two. Furthermore, the high back EMF harmonics are effectively mitigated by incurring bearable loss on the fundamental harmonic. However, the 2-D FEA would inevitably underestimate the magnitudes of cogging torque and back EMF harmonics, especially the third and fifth harmonics. Overall, satisfactory agreement was found between the synthesized 2-D and 3-D FEA results.

Comprehensive evaluation of the torque characteristics of the proposed PMSG with the two-step skewing rotor, excited by rated stator current with different phase advance angles ranging from $-30°$ to $30°$, were performed. The torque waveforms and their spectra from 2-D and 3-D FEA results are illustrated in Fig. 13. The 2-D FEA torque waveform has a very similar shape but an abated magnitude compared to its 3-D FEA counterpart. As the phase advance angle of the current mounts, the difference between 2-D and 3-D FEA results gradually diminishes as a result of magnetic saturation easing in the stator. Meanwhile, the 2-D FEA torque ripple amplitudes in most cases are substantially lower than the 3-D FEA ones as a result of the underestimated fifth harmonics of back EMF. The first harmonic components are the key contributors to the total electromagnetic torque pulsation in the machine (Fig. 13). Generally, the torque ripple amplitudes gradually decline as the phase advance angle of the current increases. Both 2-D and 3-D FEA results reveal that the machine will deliver its maximum torque at a $10°$ phase advance angle. Overall, the figures show that in most cases the 2-D FEA results will overestimate the average torque values but underestimate the torque pulsations.

Investigations on the proposed machine with three- and four-step skewing were also carried out using both the synthesized 2-D and comprehensive 3-D FEA. The resultant average torque and P-P values of torque ripple are derived and compared in Fig. 14. The average torque of the machine gradually drops and the variation in the difference between 2-D and 3-D FEA results ameliorates as the rotor skewing step number increases. This implies that the impacts of the axial air slots in the stator would be

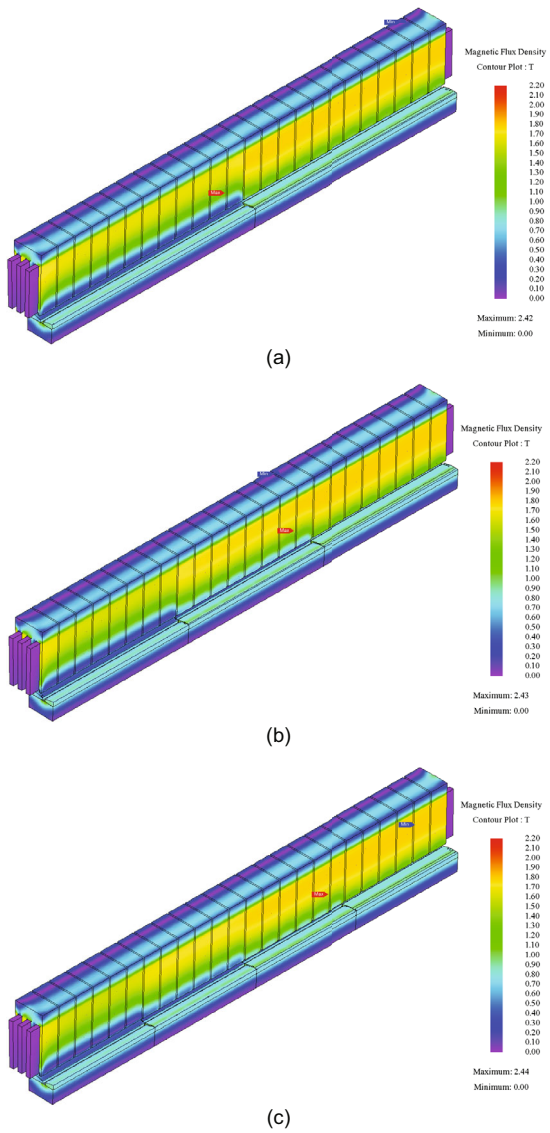

Fig. 10 3-D FEA open-circuit flux density distribution of the optimal PMSG with the rotor step skewing technique: (a) two steps; (b) three steps; (c) four steps (References to color refer to the online version of this figure)

reduced by using the rotor step skewing technique. The maximum average torque could be delivered at a current phase advance angle of 15° for machines without step skewing and 10° for machines with step skewing. Moreover, the P-P values of torque ripple in the PMSG with rotor step skewing gradually decline along with the phase advance angle of the current. The P-P torque ripple also decreases along with the number of rotor skewing steps. Note that the P-P values of torque ripple will actually increase using the step skewing technique with a current phase advance angle from −5° to 20° despite reductions in

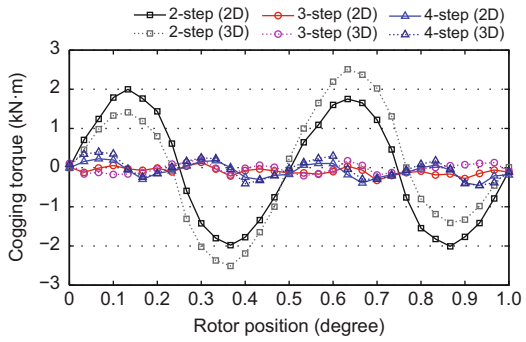

Fig. 11 Cogging torque waveforms of the machine with the rotor step skewing technique from 2-D and 3-D FEA results

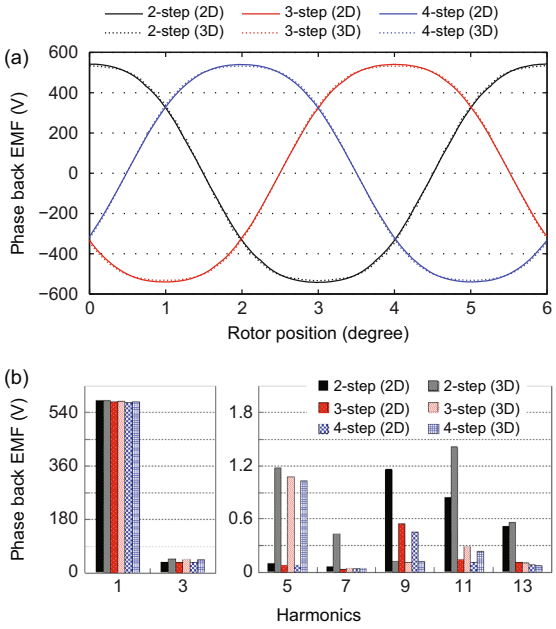

Fig. 12 2-D and 3-D FEA back EMF waveforms and spectra of the optimal machine with the step skewing technique: (a) waveforms; (b) spectra

the cogging torque and back EMF harmonics. However, there will be inevitable mechanical tolerances, which could significantly increase the cogging torque and back EMF harmonics in the proposed PMSG. Hence, the proposed rotor step skewing technique is of practical significance to minimize the torque ripple.

5 Conclusions

The torque characteristics of large low-speed direct-drive permanent magnet synchronous generators with radial ventilating air ducts in the stator for offshore wind power applications have been comprehensively investigated in this paper. Two common

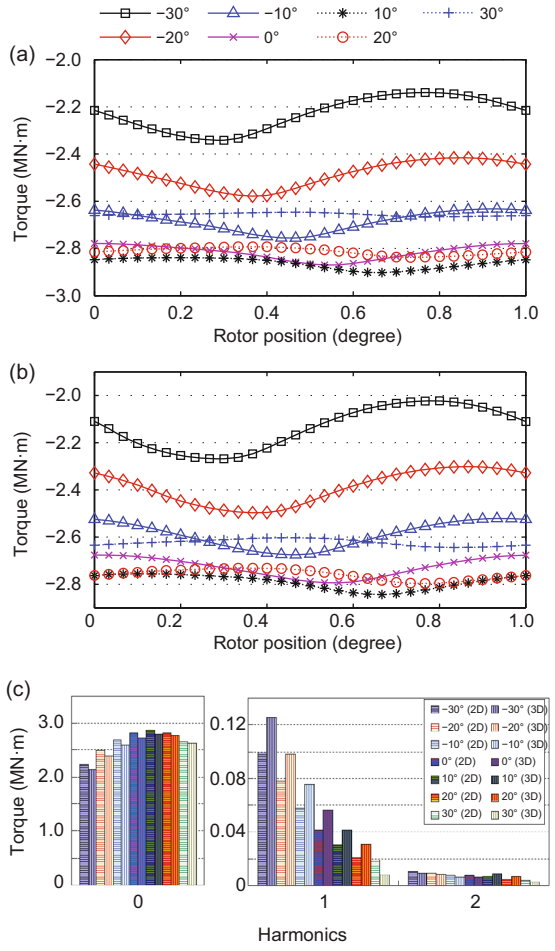

Fig. 13 2-D and 3-D FEA torque characteristics of the optimal machine with two-step skewing: (a) torque waveforms from 2-D FEA; (b) torque waveforms from 3-D FEA; (c) torque harmonic magnitudes

design techniques, magnet surface shape optimization and rotor step skewing, were implemented to improve the torque characteristics in the proposed PMSG. The conventional 2-D FEA method was used to carry out magnet shape optimization, while a comprehensive 3-D FEA method was adopted to reveal the influences of the combination of radial ventilating air ducts and rotor step skewing on the torque characteristics, including the cogging torque, torque ripple, and average torque in the machine. The results revealed that stator radial ventilating air ducts would not only reduce the average torque but also increase the torque ripple in the machine. Furthermore, the armature current phase angle and rotor skewing step number would have quite significant impacts on the reduction of the overall torque ripple in the machine. Note that the torque ripple of the machine under certain load conditions might even be

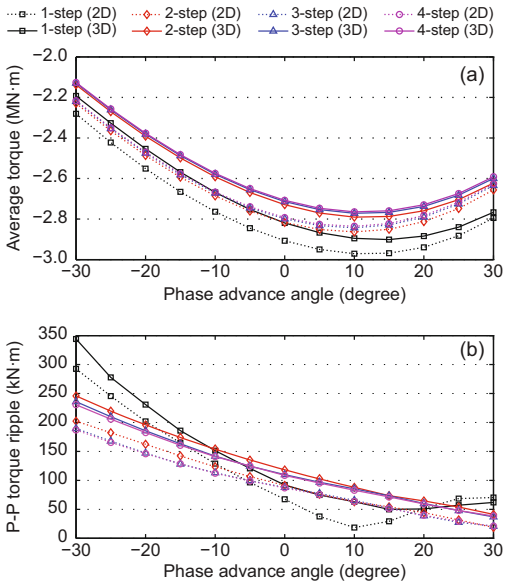

Fig. 14 2-D and 3-D FEA average torque and P-P torque ripple of the proposed machine with up to four steps: (a) average torque; (b) P-P torque ripple

increased by rotor step skewing, despite the cogging torque back EMF harmonic reduction. However, mechanical tolerances and defects are practically inevitable and impair the effectiveness of the magnet shape optimization technique. The rotor step skewing technique is a common and effective approach used to minimize the impacts of mechanical tolerances and defects and hence improve the resultant torque quality in the machine.

Acknowledgements

The authors would like to thank Powersys for software support of JMAG-Designer v12.0.

References

Ashabani, M., Mohamed, Y.A.R.I., 2011. Multiobjective shape optimization of segmented pole permanent-magnet synchronous machines with improved torque characteristics. *IEEE Trans. Magn.*, **47**(4):795-804. http://dx.doi.org/10.1109/TMAG.2010.2104327

Atallah, K., Wang, J., Howe, D., 2003. Torque-ripple minimization in modular permanent-magnet brushless machines. *IEEE Trans. Ind. Appl.*, **39**(6):1689-1695. http://dx.doi.org/10.1109/TIA.2003.818986

Bianchi, N., Bolognani, S., 2002. Design techniques for reducing the cogging torque in surface-mounted PM motors. *IEEE Trans. Ind. Appl.*, **38**(5):1259-1265. http://dx.doi.org/10.1109/TIA.2002.802989

Boukais, B., Zeroug, H., 2010. Magnet segmentation for commutation torque ripple reduction in a brushless DC motor drive. *IEEE Trans. Magn.*, **46**(11):3909-3919. http://dx.doi.org/10.1109/TMAG.2010.2057439

Chen, H.S., Dorrell, D.G., Tsai, M.C., 2010. Design and operation of interior permanent-magnet motors with two axial segments and high rotor saliency. *IEEE Trans. Magn.*, **46**(9):3664-3675. http://dx.doi.org/10.1109/TMAG.2010.2048037

Chen, N.N., Ho, S.L., Fu, W.N., 2010. Optimization of permanent magnet surface shapes of electric motors for minimization of cogging torque using FEM. *IEEE Trans. Magn.*, **46**(6):2478-2481. http://dx.doi.org/10.1109/TMAG.2010.2044764

Chu, W.Q., Zhu, Z.Q., 2013. Reduction of on-load torque ripples in permanent magnet synchronous machines by improved skewing. *IEEE Trans. Magn.*, **49**(7):3822-3825. http://dx.doi.org/10.1109/TMAG.2013.2247381

Fei, W.Z., Luk, P.C.K., 2009. An improved model for the back-EMF and cogging torque characteristics of a novel axial flux permanent magnet synchronous machine with a segmental laminated stator. *IEEE Trans. Magn.*, **45**(10):4609-4612. http://dx.doi.org/10.1109/TMAG.2009.2024127

Fei, W.Z., Luk, P.C.K., 2010. A new technique of cogging torque suppression in direct-drive permanent-magnet brushless machines. *IEEE Trans. Ind. Appl.*, **46**(4):1332-1340. http://dx.doi.org/10.1109/TIA.2010.2049551

Fei, W.Z., Luk, P.C.K., 2012. Torque ripple reduction of a direct-drive permanent-magnet synchronous machine by material-efficient axial pole pairing. *IEEE Trans. Ind. Electron.*, **59**(6):2601-2611. http://dx.doi.org/10.1109/TIE.2011.2158048

Fei, W.Z., Luk, P.C.K., Shen, J.X., 2012. Torque analysis of permanent-magnet flux switching machines with rotor step skewing. *IEEE Trans. Magn.*, **48**(10):2664-2673. http://dx.doi.org/10.1109/TMAG.2012.2198223

Fei, W.Z., Luk, P.C.K., Wu, D., *et al.*, 2013. Approximate three-dimensional finite element analysis of large permanent magnet synchronous generators with stator radial ventilating ducts. 39th Annual Conf. of IEEE Industrial Electronics Society, p.7313-7318. http://dx.doi.org/10.1109/IECON.2013.6700349

Güemes, J.A., Iraolagoitia, A.A., Del Hoyo, J.I., *et al.*, 2011. Torque analysis in permanent-magnet synchronous motors: a comparative study. *IEEE Trans. Energy Conv.*, **26**(1):55-63. http://dx.doi.org/10.1109/TEC.2010.2053374

Han, S.H., Jahns, T.M., Soong, W.L., *et al.*, 2010. Torque ripple reduction in interior permanent magnet synchronous machines using stators with odd number of slots per pole pair. *IEEE Trans. Energy Conv.*, **25**(1):118-127. http://dx.doi.org/10.1109/TEC.2009.2033196

Islam, M.S., Mir, S., Sebastian, T., *et al.*, 2005. Design consideration of sinusoidally excited permanent-magnet machines for low-torque-ripple applications. *IEEE Trans. Ind. Appl.*, **41**(4):955-962. http://dx.doi.org/10.1109/TIA.2005.851026

Islam, R., Husain, I., Fardoun, A., *et al.*, 2009. Permanent-magnet synchronous motor magnet designs with skewing for torque ripple and cogging torque reduction. *IEEE Trans. Ind. Appl.*, **45**(1):152-160. http://dx.doi.org/10.1109/TIA.2008.2009653

Jahns, T.M., Soong, W.L., 1996. Pulsating torque minimization techniques for permanent magnet AC motor drives—a review. *IEEE Trans. Ind. Electron.*, **43**(2):321-330. http://dx.doi.org/10.1109/41.491356

Lateb, R., Takorabet, N., Meibody-Tabar, F., 2006. Effect of magnet segmentation on the cogging torque in surface-mounted permanent-magnet motors. *IEEE Trans. Magn.*, **42**(3):442-445. http://dx.doi.org/10.1109/TMAG.2005.862756

Li, T., Slemon, G., 1988. Reduction of cogging torque in permanent magnet motors. *IEEE Trans. Magn.*, **24**(6):2901-2903. http://dx.doi.org/10.1109/20.92282

Pang, Y., Zhu, Z.Q., Howe, D., 2005. Self-shielding magnetized vs. shaped parallel-magnetized PM brushless AC motors. *KIEE Int. Trans. Electr. Mach. Energy Conv. Syst.*, **5-B**(1):13-19.

Pyrhonen, J., Ruuskanen, V., Nerg, J., *et al.*, 2010. Permanent-magnet length effects in AC machines. *IEEE Trans. Magn.*, **46**(10):3783-3789. http://dx.doi.org/10.1109/TMAG.2010.2050002

Ruuskanen, V., Nerg, J., Pyrhonen, J., 2011. Effect of lamination stack ends and radial cooling channels on no-load voltage and inductances of permanent-magnet synchronous machines. *IEEE Trans. Magn.*, **47**(11):4643-4649. http://dx.doi.org/10.1109/TMAG.2011.2158233

Ruuskanen, V., Nerg, J., Niemelä, M., *et al.*, 2013. Effect of radial cooling ducts on the electromagnetic performance of the permanent magnet synchronous generators with double radial forced air cooling for direct-driven wind turbines. *IEEE Trans. Magn.*, **49**(6):2974-2981. http://dx.doi.org/10.1109/TMAG.2013.2238679

Sopanen, J., Ruuskanen, V., Nerg, J., *et al.*, 2011. Dynamic torque analysis of a wind turbine drive train including a direct-driven permanent-magnet generator. *IEEE Trans. Ind. Electron.*, **58**(9):3859-3867. http://dx.doi.org/10.1109/TIE.2010.2087301

Tapia, J.A., Pyrhonen, J., Puranen, J., *et al.*, 2013. Optimal design of large permanent magnet synchronous generators. *IEEE Trans. Magn.*, **49**(1):642-650. http://dx.doi.org/10.1109/TMAG.2012.2207907

Wang, Y., Jin, M.J., Fei, W.Z., *et al.*, 2010. Cogging torque reduction in permanent magnet flux-switching machines by rotor teeth axial pairing. *IET Electr. Power Appl.*, **4**(7):500-506. http://dx.doi.org/10.1049/iet-epa.2009.0205

Yang, Y., Wang, X., Zhang, R., *et al.*, 2006. The optimization of pole arc coefficient to reduce cogging torque in surface-mounted permanent magnet motors. *IEEE Trans. Magn.*, **42**(4):1135-1138. http://dx.doi.org/10.1109/TMAG.2006.871452

Zhu, Z.Q., Howe, D., 2000. Influence of design parameters on cogging torque in permanent magnet machines. *IEEE Trans. Energy Conv.*, **15**(4):407-412. http://dx.doi.org/10.1109/60.900501

Zhu, Z.Q., Ruangsinchaiwanich, S., Ishak, D., *et al.*, 2005. Analysis of cogging torque in brushless machines having nonuniformly distributed stator slots and stepped rotor magnets. *IEEE Trans. Magn.*, **41**(10):3910-3912. http://dx.doi.org/10.1109/TMAG.2005.854968